Entrainment and small-scale features in merging turbulent regions

Journal of Physics: Conference Series **3173** (2026) 012025 doi:10.1088/1742-6596/3173/1/012025

Entrainment and small-scale features in merging turbulent regions

Francisco A. Branco[1], Andrea Cimarelli[2] and Carlos B. da Silva[1]

[1]IDMEC/Instituto Superior Técnico, University of Lisbon, Lisbon, Portugal
[2]DIEF, University of Modena and Reggio Emilia, Modena, Italy

E-mail: franciscoabranco@tecnico.ulisboa.pt

Abstract. The small-scale structure of turbulent/non-turbulent interfaces (TNTIs) that develop between two merging turbulent regions is investigated using direct numerical simulations. The study is based on a canonical flow configuration in which two homogeneous and isotropic turbulent (HIT) fronts, initially separated by an irrotational region, evolve spatially with no imposed mean shear. To generate realistic inlet conditions, we use velocity fields from temporally-evolving HIT simulations, computed with spectral accuracy, which are spatially advected by a uniform mean velocity field. The non-turbulent core is created by applying a smoothing hyperbolic tangent filter to the velocity fields, which effectively removes the fluctuations in the inner region. As the turbulent fronts evolve, they entrain irrotational fluid, interact, and eventually merge. During this process, the conditional mean enstrophy, which initially matches that of a classical TNTI, begins to depart from its universal shape. The interaction between the two turbulent regions influences the smallest scales near the TNTI, leading to a flow that is locally more homogeneous compared to the classical case. The local entrainment velocity remains nearly constant during merging, despite extreme detrainment events becoming increasingly rare in the downstream direction. This suggests the existence of significant changes in the geometry of the irrotational boundary as the merging progresses.

1 Introduction

The merging of turbulent regions occurs in a wide variety of flows in engineering. Straightforward examples include wind farms, where the wakes of turbines upstream interact and merge, affecting the operation of downstream turbines and contribute to power losses [1]. In non-premixed reacting flows, it is known that the efficiency depends on the turbulent mix between the streams that supply fuel and oxidizer [2]. Besides these evident examples, the physical coalescence of turbulent regions can potentially be interpreted as the interaction or collision of vortices (the fundamental constituents of turbulence), which is considered to be one of the dominant sources of aeroacoustic noise in various canonical turbulent flows [3, 4].

In spite of the strong interest in this flow, few studies have discussed the structure of turbulent/turbulent merging (TTM), even in its simplest form - without mean shear. While interacting jets and wakes have been examined more extensively [5, 6], a detailed description of the small-scale structure of the developing TNTIs in these flows is lacking. Such descriptions are essential not only for understanding turbulent entrainment (relevant to many engineering applications) but the analysis of small-scales in such configuration is also interesting for advancing the study of energy cascades under out-of-equilibrium conditions, which have been observed in these flows [5].

In this work, we have performed direct numerical simulations (DNS) of merging turbulent fronts without mean shear and analysed the evolution of small-scales conditioned to the TNTIs during the growth of the turbulent streams, their mutual interaction and actual merging. The dataset of DNS adopts an inlet condition, where results from a precursor DNS are imposed, guaranteeing physical realism (§2.2). The detection of the TNTIs is depicted in §2.3 and the analysis of the conditional profiles is presented in §3. Implications on the local entrainment velocity are discussed (§3), and the main conclusions are withdrawn in §4.

2 Numerical methods

2.1 Spatial and temporal discretisation

The governing equations, i.e. incompressible Navier-Stokes in Cartesian coordinates, are solved numerically with a pseudo-spectral and compact finite differences code (see [7] and references therein). The domain is a three dimensional box, where the streamwise (x) dimension is three times larger than the normal (y) and spanwise (z) lengths in order to fully accommodate the merging region of the turbulent fronts. The grid spacings, $\Delta x = \Delta y = \Delta z$, are uniform. The spatial discretisation of the equations is performed with a sixth-order-compact scheme [8] in the streamwise direction, x, and pseudo-spectral methods are employed in the normal, y, and spanwise, z directions, with de-aliasing done with the 2/3rd rule.

The temporal advancement is performed with a third-order low storage explicit Runge–Kutta time-stepping scheme [9], combined with a fractional step method that ensures pressure-velocity coupling and incompressibility at each substep of the time-advancing scheme [10]. At the outlet, a non-reflective outflow condition is employed, which guarantees minimum distortion of the pressure field is achieved and the coherent structures leave the computational domain without being affected [11]. The normal and spanwise directions are periodic. The inflow condition is specified in the following section.

2.2 Inflow condition

The inlet condition adopted in the present work is a variation of the ones previously implemented to simulate a temporal shearless mixing layer [12]. The underlying idea is to impose at the inlet velocity fluctuations that are extracted from a separate temporal forced homogenous isotropic turbulence (HIT) simulation. This guarantees that the fluctuating velocity fields injected at the inlet are a solution of the NSE and follow the characteristic energy spectrum of isotropic turbulence.

The procedure by which these velocity fluctuations are introduced on the spatial domain can be conceptually divided in three steps: i) at each iteration, the instantaneous $y-z$ velocity plane located at the middle of the triperiodic cube is extracted, generating planes with the fluctuating components of the velocity field, $u'(y,z)$, $v'(y,z)$ and $w'(y,z)$; ii) then, a non-turbulent region with thickness H is created by convolving the u', v', and w' HIT planes with a hyperbolic tangent profile, see equation (1), setting to zero the velocity fluctuations in the core region; iii) the final step is the addition of a uniform convection velocity, U_∞, to the modified HIT plane.

The combination of these steps can be written as

$$\begin{aligned} u(x=0,y,z) &= U_\infty + u'(y,z)\left[\frac{1}{2}\left(1-\tanh\left[\frac{1}{a}\left(1-\frac{2|y|}{H}\right)\right]\right)\right], \\ v(x=0,y,z) &= v'(y,z)\left[\frac{1}{2}\left(1-\tanh\left[\frac{1}{a}\left(1-\frac{2|y|}{H}\right)\right]\right)\right], \\ w(x=0,y,z) &= w'(y,z)\left[\frac{1}{2}\left(1-\tanh\left[\frac{1}{a}\left(1-\frac{2|y|}{H}\right)\right]\right)\right], \end{aligned} \tag{1}$$

where u', v' and w' are the velocity components extracted from the HIT simulation, while u, v, and w are the instantaneous velocities at the inlet, $x=0$. The parameter H is the initial width of the non-turbulent region (where velocity fluctuations are set to zero), and a is a parameter that regulates the gradient of the convolution profile. Note that as $a \to 0$, the hyperbolic tangent profile approximates to a boxed shape, which contaminates the flowfield with spurious oscillations (Gibbs phenomena). In turn, if a is large the convolution profile smooths the otherwise very sharp TNTI, losing physical realism. We have set $1/a = 20$, which yields a good compromise between these two conflicting effects. It is smooth enough not to introduce numerical noise, while being sufficiently sharp to represent the TNTI (the steep filtering is localised within $\sim 0.1H \approx 12\eta$, matching the actual thickness of a classical TNTI [13]).

The present method offers an unprecedented level of control over the properties of the two turbulent streams. Starting from an initial temporal HIT simulation, we can virtually tailor the energy spectrum

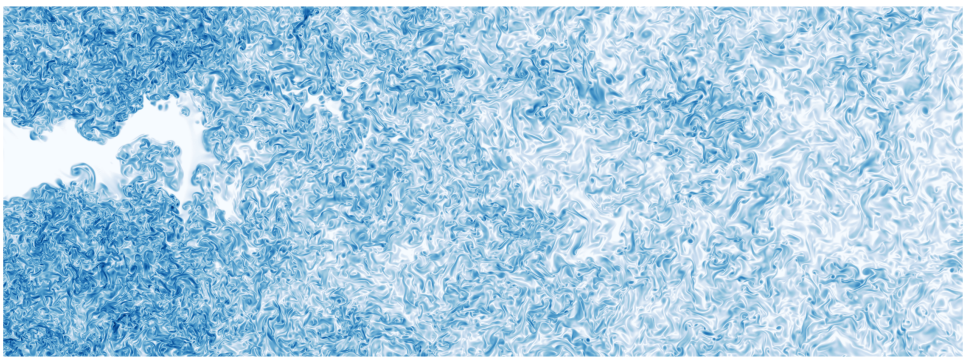

Figure 1: Contours of vorticity magnitude (in logarithmic scale) sampled at a given instant of time at the central $x-y$ plane. Values are normalised by the freestream velocity U_∞ and the non-turbulent slot-width H. The region represented spans from $-3 \leq y/H \leq 3$ and $1.5 \leq x/H \leq 18$.

to a desired shape. By setting the peak location, we define the integral scale, while adjusting the forcing power controls the level of turbulent kinetic energy. Moreover, the addition of a convection velocity when injecting the modified HIT plane into the spatial simulation allows us to set the desired turbulence intensity. This new inflow condition opens up entirely new possibilities for simulating turbulent/turbulent merging. A visualization of the resulting flowfield is presented in figure 1.

2.3 Interface detection

Conditional statistics are employed here due to the difficulty of capturing the dynamics of the turbulent/non-turbulent interface (TNTI) using a fixed reference frame. By conditioning on the distance from the TNTI, we can clearly separate turbulent and irrotational regions of the flow, preserving important flow features that would otherwise be blurred in the statistics, due the the addition of turbulent and non-turbulent flow data. The procedure for computing these conditional statistics is as follows: i) the outer edge of the TNTI, referred to as the irrotational boundary (IB), is defined as an iso-surface of low vorticity magnitude; ii) at each point of the IB, a local normal axis y_I is established, with its origin at the IB. This normal points in the direction of the enstrophy gradient, so that $y_I > 0$ corresponds to rotational (turbulent) fluid, and $y_I < 0$ to irrotational fluid; iii) flow quantities are interpolated along these local normal directions, and the statistics are accumulated as a function of distance y_I from the IB. This conditional averaging is denoted by $\langle\cdot\rangle_I$.

In this work, due to the complex geometry of the interface during the merging process, we use the actual IB surface rather than the more conventional interface envelope [14]. This choice allows for the inclusion of interface re-entrances in the statistical sampling, resulting in more accurate and representative statistics.

Since the flow is spatially decaying (note that the turbulent streams evolve without mean shear) the calculated threshold of vorticity magnitude to locate the IB will depend on the streamwise location. In this sense, and to study the local TNTI evolution during merging, the merging region is divided in thin slabs of thickness $0.5H$ in the streamwise direction. In total, nine slabs are analysed. The threshold is maintained for each slab (allowing to track entrainment), but is recalculated for the different streamwise positions covered. For the remainder of this paper, each slab is assigned a different colour: lighter colours correspond to slabs further downstream.

3 Results

The so-called classical turbulent/non-turbulent interface (TNTI), observed in a wide range of flows, has been the focus of numerous previous studies [15, 16, 17]. This interface between irrotational and turbulent regions is notably sharp, typically spanning over a narrow layer on the order of a few Kolmogorov microscales (approximately 12η). As a result, the conditional enstrophy profile exhibits a marked discontinuity at the interface boundary (IB).

Within this narrow layer of roughly 12η, the TNTI is commonly divided into two distinct subregions, each characterized by different physical mechanisms. In the very close proximity of the IB, diffusive mechanisms are predominant (the only way an irrotational fluid portion can become rotational is by viscous diffusion of enstrophy), hence this very thin viscous region (that spans $\langle\delta_\nu\rangle \approx 3-4\eta$) is termed *viscous*

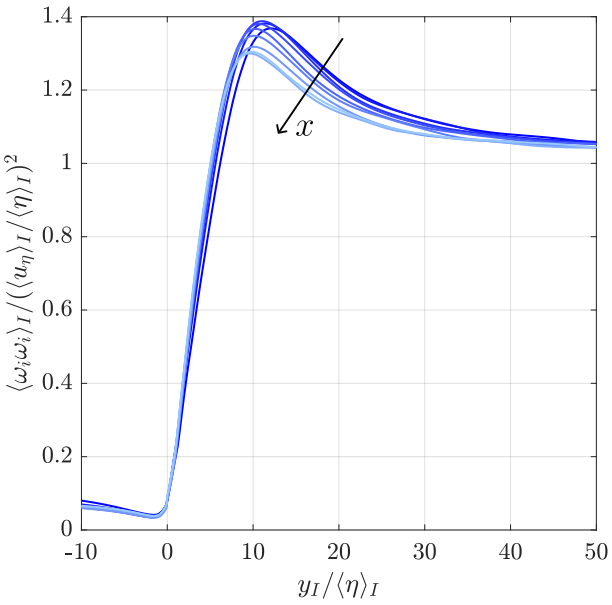

Figure 2: Conditional mean enstrophy profiles during merging, normalised by local Kolmogorov scales [14]. Lighter colours represent increasing streamwise distance, i.e. the direction of merging (as denoted by the arrow).

superlayer (VSL) [18]. Further inside the turbulent core, enstrophy has already become non-negligible, by the diffusive action of the VSL, and production by vortex stretching becomes the predominant mechanism for the enstrophy growth within the TNTI. This layer is termed *turbulent sublayer* (TSL) and has a thickness of $\langle\delta_T\rangle \approx 8-10\eta$.

It has been shown that, when properly normalised, the small-scales within the TNTI are universal. Specifically, after enstrophy is non-dimensionalised by local Kolmogorov timescales, their profiles collapse irrespective of the flow in consideration [14]. We note that this normalisation expresses a local comparison between the magnitudes of rotational and straining motions, which, on average, are known to be equal for homogeneous turbulent flows [19]. Figure 2 presents the conditional evolution of enstrophy under this normalisation, for the different slabs analysed, before and during merging in the present configuration.

In contrast to a classical TNTI, there is a clear streamwise dependence of the profiles. Sufficiently upstream of the merging point, the evolution of conditional enstrophy collapses satisfactorily, with the value and location of the peak being in accordance with results from 'classical' TNTIs. However, as the two turbulent streams approach each other, they start to interact and the peak decreases in intensity and is slightly displaced towards the IB. Hence, the interaction is felt at the smallest scales very close to the TNTI and can be interpreted as a local homogenisation of the flow. To see this, consider the normalised enstrophy written as

$$\left\langle \frac{\omega_i\omega_i}{(u_\eta/\eta)^2} \right\rangle_I = \frac{\langle(\partial u_i/\partial x_j)^2\rangle_I - \langle(\partial u_i/\partial x_j)(\partial u_j/\partial x_i)\rangle_I}{\langle(\partial u_i/\partial x_j)^2\rangle_I + \langle(\partial u_i/\partial x_j)(\partial u_j/\partial x_i)\rangle_I}. \tag{2}$$

The term $\langle(\partial u_i/\partial x_j)(\partial u_j/\partial x_i)\rangle$ that appears in the numerator and denominator with opposite signs is identically null in homogenous turbulence [20]. Therefore, values of normalised enstrophy larger than one (as occurs in the peak), are a consequence of $\langle(\partial u_i/\partial x_j)(\partial u_j/\partial x_i)\rangle < 0$, i.e. inhomogeneity. Hence, the decreasing intensity of the peak can be interpreted as a local small-scale homogenisation at the border of the TNTI during merging. Only sufficiently away from the TNTI ($\approx 50\eta$) the flow reattains homogeneity. A discussion of the causes behind this homogenisation is postponed to a later paper. For now, we will focus on its potential effects to turbulent entrainment.

In fact, since the interacting streams alter the small-scale organization within the TNTI and posing that small-scale nibbling is the dominant contribution for entrainment, some variations are to be expected in the present flow configuration, when compared to entrainment in usual TNTIs. We have calculated

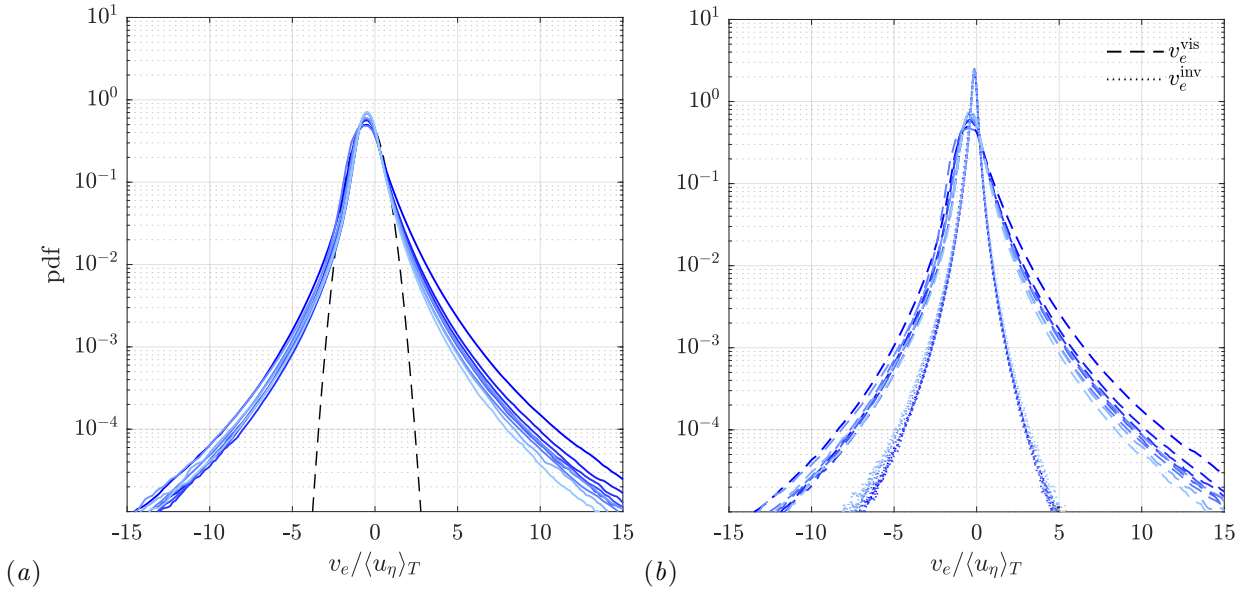

Figure 3: Probability density function (PDF) of (a) the entrainment velocity, v_e, and (b) its viscous and inviscid components, v_e^{vis}, and v_e^{inv}, respectively.

the local entrainment velocity [18, 21],

$$v_e = -\underbrace{\frac{2\omega_i\omega_j S_{ij}}{|\nabla(\omega_i\omega_i)|}}_{v_e^{\mathrm{inv}}} \underbrace{-\frac{\nu\nabla^2(\omega^2)}{|\nabla(\omega_i\omega_i)|} + \frac{2\nu(\boldsymbol{\nabla}\omega_i\cdot\boldsymbol{\nabla}\omega_i)}{|\nabla(\omega_i\omega_i)|}}_{v_e^{\mathrm{vis}}}, \tag{3}$$

for the different slabs analysed. The terms on the right-hand side are evaluated at the IB and can be grouped into an inviscid contribution (from enstrophy production by vortex stretching) and a viscous one (from the combined effect of diffusion and dissipation).

As shown in figure 3, displaying the probability density function (PDF) of v_e throughout merging, there is a preference for $v_e < 0$, that in our convention denotes entrainment events, i.e. the ingestion of irrotational fluid by the turbulent streams. Its average value is found to be insensitive to the downstream position, being $\langle v_e \rangle \sim \mathcal{O}(u_\eta)$ for every slab analysed.

The distinct wide tails of v_e are evident when compared to a Gaussian distribution (dashed line in figure 3). The probability of $v_e < 0$ (entrainment) remains slightly unchanged during merging, as opposed to detrainment ($v_e > 0$), that is found to decrease downstream. Comparing the PDF of the inviscid and viscous terms in (3), the reduction of $v_e > 0$ can be attributed to v_e^{vis}, that mainly acts at the smallest scales, as attested by its wider tails that arise from the small-scale intermittency. We note that the PDF of the inviscid contribution is negatively skewed, confirming the preference for vortex stretching rather than compression, and its shape remains unchanged as the two turbulent regions mix.

Previous works have pointed a correlation between entrainment/detrainment and the local curvature of the TNTI [18]. From this perspective, the decreasing positive tail of v_e may suggest a change on the geometry of the TNTI. In sum, the mixing between the turbulent layers creates pockets of irrotational fluid whose properties differ from 'classical' TNTIs: there is a more homogenous flow within the TNTI and the decreasing probability of detrainment events is indicative of changes on how irrotational fluid is organised.

4 Conclusions

This paper discusses some aspects of small-scales and entrainment in merging turbulent regions. We have conducted new spatially-developing direct numerical simulations especially tailored for this study. A shearless merging of two turbulent streams is achieved by using a new inlet condition that advects velocity planes, calculated with spectral accuracy, from a separate temporal DNS. Some advantages of this inflow prescription are highlighted, namely its physical realism, resulting in an almost full exploitation of the entire spatial domain, and the great level of control over the turbulence parameters desired.

Conditional mean profiles in relation to the distance from the irrotational boundary that forms while the two turbulent streams merge are presented. These statistics are obtained using a three-dimensional normal distance to the irrotational boundary. Different streamwise locations with respect to the merging point are analysed in order to address the evolution of entrainment and small-scales along the merging region.

Results suggest slight but considerable deviations of the small-scale properties of the TNTIs in the merging region when compared to 'classical' ones (such those in jets, wakes, or boundary layers sufficiently isolated from other turbulent streams). One apparent contrast is the decreasing normalised enstrophy peak that delimits the TNTI. In this view, the mixing of two turbulent streams can be interpreted as a local homogenisation of the turbulence boundary, resulting from the interaction between the adjacent turbulent streams. The average entrainment velocity remains approximately constant, but there is reduction of detrainment events in the merging region. The causes behind this homogenisation and apparent consequences on the geometry of the TNTIs that appear in this intense mixing region will be assessed in the near future.

Acknowledgements. The authors acknowledge Minho Advanced Computing Center for providing HPC computing and consulting resources that have contributed to the research results reported within this paper (https://macc.fccn.pt). The authors also acknowledge the Laboratory for Advanced Computing at University of Coimbra for providing HPC, computing and consulting resources (http://www.lca.uc.pt).

Funding. The authors acknowledge Fundação para a Ciência e Tecnologia (FCT) for its financial support via the project LAETA Base Funding (DOI: 10.54499/UIDB/50022/2020). F.A.B. acknowledges Fundação para a Ciência e Tecnologia (FCT) for the scholarship 2025.02332.BD (DOI: 10.54499/2025.02332.BD). C.B.S. acknowledges Fundação para a Ciência e Tecnologia (FCT) for its financial support via projects DOI: 10.54499/2023.15779.PEX, and DOI: 10.54499/2023.14450.CPCA.A3.

References

[1] Haohua Zong and Fernando Porté-Agel. A momentum-conserving wake superposition method for wind farm power prediction. *Journal of Fluid Mechanics*, 889:A8, 2020.

[2] R.W. Bilger. Turbulent jet diffusion flames. In *Energy and Combustion Science*, pages 109–131. Pergamon, 1979.

[3] S. Kida, M. Takaoka, and F. Hussain. Collision of two vortex rings. *Journal of Fluid Mechanics*, 230:583–646, 1991.

[4] Hamid Daryan, Fazle Hussain, and Jean-Pierre Hickey. Aeroacoustic noise generation due to vortex reconnection. *Phys. Rev. Fluids*, 5:062702, Jun 2020.

[5] J.G. Chen, C. Cuvier, J.-M. Foucaut, Y. Ostovan, and J.C. Vassilicos. A turbulence dissipation inhomogeneity scaling in the wake of two side-by-side square prisms. *Journal of Fluid Mechanics*, 924:A4, 2021.

[6] Fanny Olivia Johannessen Berstad, R. Jason Hearst, and Ingrid Neunaber. Wake merging and turbulence transition downstream of side-by-side porous discs. *Journal of Fluid Mechanics*, 1015:A39, 2025.

[7] Mateus C. Guimarães, Fernando T. Pinho, and Carlos B. da Silva. Turbulent planar wakes of viscoelastic fluids analysed by direct numerical simulations. *Journal of Fluid Mechanics*, 946:A26, 2022.

[8] Sanjiva K. Lele. Compact finite difference schemes with spectral-like resolution. *Journal of Computational Physics*, 103(1):16–42, 1992.

[9] J.H Williamson. Low-storage Runge-Kutta schemes. *Journal of Computational Physics*, 35(1):48–56, 1980.

[10] J. Kim and P. Moin. Application of a fractional-step method to incompressible Navier-Stokes equations. *Journal of Computational Physics*, 59(2):308–323, 1985.

[11] I. Orlanski. A simple boundary condition for unbounded hyperbolic flows. *Journal of Computational Physics*, 21(3):251–269, 1976.

[12] Andrea Cimarelli, Giacomo Cocconi, Bettina Frohnapfel, and Elisabetta De Angelis. Spectral enstrophy budget in a shear-less flow with turbulent/non-turbulent interface. *Physics of Fluids*, 27(12):125106, 12 2015.

[13] Tiago S. Silva, Marco Zecchetto, and Carlos B. da Silva. The scaling of the turbulent/non-turbulent interface at high Reynolds numbers. *Journal of Fluid Mechanics*, 843:156–179, 2018.

[14] Marco Zecchetto and Carlos B. da Silva. Universality of small-scale motions within the turbulent/non-turbulent interface layer. *Journal of Fluid Mechanics*, 916:A9, 2021.

[15] David K. Bisset, Julian C. R. Hunt, and Michael M. Rogers. The turbulent/non-turbulent interface bounding a far wake. *Journal of Fluid Mechanics*, 451:383–410, 2002.

[16] J. Westerweel, C. Fukushima, J. M. Pedersen, and J. C. R. Hunt. Mechanics of the turbulent-nonturbulent interface of a jet. *Phys. Rev. Lett.*, 95:174501, 2005.

[17] Kapil Chauhan, Jimmy Philip, Charitha M. de Silva, Nicholas Hutchins, and Ivan Marusic. The turbulent/non-turbulent interface and entrainment in a boundary layer. *Journal of Fluid Mechanics*, 742:119–151, 2014.

[18] M. Holzner and B. Lüthi. Laminar superlayer at the turbulence boundary. *Phys. Rev. Lett.*, 106:134503, 2011.

[19] R. Betchov. An inequality concerning the production of vorticity in isotropic turbulence. *Journal of Fluid Mechanics*, 1(5):497–504, 1956.

[20] G.I. Taylor. The spectrum of turbulence. *Proc. Math. Phys. Eng. Sci.*, 164(919):476–490, 1938.

[21] M. Wolf, B. Lüthi, M. Holzner, D. Krug, W. Kinzelbach, and A. Tsinober. Investigations on the local entrainment velocity in a turbulent jet. *Physics of Fluids*, 24(10):105110, 2012.